



Research article

Based on the prognosis model of immunogenes, the prognosis model was constructed to predict the invasion of immune genes and immune cells related to primary liver cancer and its experimental validation

Yu-Ping Yang^{a,1}, Min Bai^{a,1}, Yin-Xia Cheng^{b,1}, Xin Feng^a, Yan-Ying Zhang^a, Yuan-Yuan Zhang^a, Meng-Ya Liu^a, Yong-Qiang Duan^{b,*}

^a Gansu University of Traditional Chinese Medicine, College of Basic Medical Sciences, Lanzhou, 730000, PR China

^b Ningxia Medical University, College of Traditional Chinese Medicine, Yinchuan, 750000, PR China

ARTICLE INFO

Keywords:

Primary liver cancer
Immune-related gene pair
Immune-related gene
Immune cell
Experimental validation

ABSTRACT

Background: Primary liver cancer (PLC) is a prevalent malignancy of the digestive system characterized by insidious symptom onset and a generally poor prognosis. Recent studies have highlighted a significant correlation between the initiation and prognosis of liver cancer and the immune function of PLC patients.

Purpose: Revealing the expression of PLC-related immune genes and the characteristics of immune cell infiltration provides assistance for the analysis of clinical pathological parameters and prognosis of PLC patients.

Methods: PLC-related differentially expressed genes (DEGs) with a median absolute deviation (MAD > 0.5) were identified from TCGA and GEO databases. These DEGs were intersected with immune-related genes (IRGs) from the ImmPort database to obtain PLC-related IRGs. The method of constructing a prognostic model through immune-related gene pairs (IRGPs) is used to obtain IRGPs and conduct the selection of central immune genes. The central immune genes obtained from the selection of IRGPs are validated in PLC. Subsequently, the relative proportions of 22 types of immune cells in different immune risk groups are evaluated, and the differential characteristics of PLC-related immune cells are verified through animal experiments.

Results: Through database screening and the construction of an IRGP prognosis model, 84 pairs of IRGPs ($P < 0.001$) were ultimately obtained. Analysis of these 84 IRGPs revealed 11 central immune genes related to PLC, showing differential expression in liver cancer tissues compared to normal liver tissues. Results from the CiberSort platform indicate differential expression of immune cells such as naive B cells, macrophages, and neutrophils in different immune risk groups. Animal experiments demonstrated altered immune cell proportions in H22 tumor-bearing mice, validating findings from peripheral blood and spleen homogenate analyses.

Conclusion: Our study successfully predicted and validated PLC-related IRGs and immune cells, suggesting their potential as prognostic indicators and therapeutic targets for PLC.

* Corresponding author.

E-mail address: dyqgs2008@163.com (Y.-Q. Duan).

¹ These authors have equally contribution.

<https://doi.org/10.1016/j.heliyon.2024.e27362>

Received 1 September 2023; Received in revised form 28 February 2024; Accepted 28 February 2024

Available online 16 March 2024

2405-8440/© 2024 Published by Elsevier Ltd.

This is an open access article under the CC BY-NC-ND license

(<http://creativecommons.org/licenses/by-nc-nd/4.0/>).

1. Introduction

Liver cancer is the most prevalent lethal malignancy globally, ranking as the fourth most common malignancy and second-leading cause of cancer-related deaths in China [1,2]. The annual incidence of liver cancer in China contributes to 35.5% of global morbidity [2,3]. Major risk factors include hepatitis B and C viruses, fatty liver, alcoholic cirrhosis, smoking, obesity, diabetes mellitus, iron overload, and exposure to aflatoxin-contaminated food [4,5]. Modern medical research [2] suggested that liver cancer can not be identified by the pain feedback mechanism. When diagnosed, most liver cancer patients already present with advanced-stage disease. Despite progress in systemic treatments such as surgery and molecular-targeted drugs, challenges such as late diagnosis, chemo-resistance, recurrence, and frequent metastasis persist, leading to poor prognoses for liver cancer [6]. Despite continuous updates in new drug development and treatment strategies in recent years, their impact on liver cancer treatment has been limited [7,8]. Urgent attention is required to address the medical challenge of developing new therapeutic strategies for liver cancer.

The liver, as an immune-privileged organ, harbors diverse immunocompetent cells, including Kupffer cells (KCs), liver sinusoidal endothelial cells (LSECs), and lymphocytes. These cells actively engage in immune responses through the intricate processes of blood circulation and metabolism in the hepatic artery and hepatic portal vein. The liver's unique immunological tolerance to antigens involves a delicate balance achieved through primary T cell activation and immunosuppressive mechanisms, ultimately exerting a finely tuned immunological effect [9,10]. However, traditional treatments such as surgical resection, radiofrequency ablation, and transarterial chemoembolization (TACE), while targeting the cancer itself, inflict considerable damage to both liver function and overall immunity. Chronic liver injury induced by viruses or drugs further impairs systemic and local immune microenvironment-regulating mechanisms, contributing to the increased spread and metastasis of cancer. Consequently, liver cancer patients face dismal prognoses characterized by a low 5-year survival rate [11]. In recent years, based on microarray and RNA-sequencing methods, there have been increasing studies on immune-related prognostic signatures in human cancers [12–15]. For example, using a cohort of glioma samples with expression information from whole-genome microarrays from the Chinese Glioma Genome Atlas and TCGA databases, researchers constructed a local risk signature associated with immunity that can independently identify patients with a high risk [16]. Wang et al. [17] used the TCGA and ImmPort databases to build a 15-gene prognostic model in renal papillary cell carcinoma. Their signature was associated with tumor staging and tumor type. Furthermore the rapid development of immunotherapy has revolutionized cancer treatment, including liver cancer. Immunotherapy, designed to bolster the immune system's activity against cancer cells, has introduced novel therapeutic approaches [18,19]. Agents like sorafenib, lenvatinib, regorafenib, cabozantinib, and the vascular endothelial growth factor (VEGF) inhibitor [20] ramucirumab are now integral to tumor immunotherapy, serving as first-line treatments for liver cancer. However, challenges persist, with inadequate evidence on drug resistance, treatment response prediction, and suboptimal efficacy in liver cancer treatment. Consequently, there is an urgent need to explore new therapeutic strategies and identify prognostic biomarkers for liver cancer. Despite the recognized significance of cancer biomarkers in predicting survival and guiding disease control and prevention, biomarkers specifically related to immune genes in liver cancer remain unexplored. Leveraging data from The Cancer Genome Atlas (TCGA) and Gene Expression Omnibus (GEO) databases, this study systematically selected liver cancer-related immune-related genes (IRGs) and immune cells. Through comprehensive analysis and experimental validation, a novel protocol for understanding and addressing liver cancer is presented, offering potential avenues for enhanced therapeutic strategies and biomarker identification.

2. Methods

2.1. Prediction of PLC-related hub IRGs and infiltrative immune cells

2.1.1. PLC-related data acquisition and preprocessing

In this study, transcriptome data of liver cancer were initially downloaded from the Tumor Genome Atlas (TCGA) database. Perl data collation was utilized to extract expression data of liver cancer, with the data type being Fragments Per Kilobase Million (FPKM). Standardized processing and differential analysis were performed using the limma package of R4.2.1 software, with differential genes identified based on criteria of $|\log_{2}FC| > 1$ and corrected P value < 0.05 . Subsequently, liver cancer chip sequencing data were obtained from the GEO database, specifically using the GSE76427 dataset. The chip probe ID file and the expression matrix were downloaded, and perl scripting was applied to convert probe IDs in the expression matrix file into corresponding gene names. Differential analysis was carried out using the limma package of R4.2.1 software, with differential genes identified using the criteria of $|\log_{2}FC| > 1$ and corrected P value < 0.05 . The identified differential genes from TCGA and GEO datasets were then subjected to an intersection analysis, and the common genes were considered as the differential genes associated with liver cancer. Finally, the intersection of these liver cancer-related differential genes with IRGs from The Immunology Database and Analysis Portal (ImmPort) database was performed to obtain immune-related hepatoma differential genes.

2.1.2. Acquisition of PLC-related IRGs

IRGs from TCGA and GEO databases were selected based on a median absolute deviation (MAD) greater than 0.5. Additionally, immune-related gene pairs (IRGPs) were calculated by comparing gene expression levels in specific samples in pairs. In a specific IRGP, if the expression level of the first IRG is higher than that of the second IRG, the score of the IRGP is 1; Otherwise, the score is 0. If the score of IRGP is 0 or 1 in more than 80% or less than 20% of TCGA data set, the IRGP will not be employed, and the remaining IRGPs will be reserved as initial candidates for subsequent analysis. Select prognosis-related IRGP [false

discovery rate (FDR) < 0.01] in TCGA data set, and use R software package (glmnet) for Lasso Cox proportional hazard regression (iteration number = 1000) and 10-fold cross-validation to calculate immune-related gene pairs index (IRGPI), and obtain (4135 * 400). After removing samples with gene pair value of 0 or 1 and samples with gene pair Pvalue \geq 0.05 from all data sets, the remaining IRGPs (84 pairs of IRGP) were used to construct the prognosis model.

2.1.3. IRGP prognostic model construction and PLC hub IRG selection

Through Lasso regression, 84 IRGP pairs were further obtained to obtain 29 IRGP and their regression coefficients. The optimal cut-off for IRGPI was determined using the receiver operating characteristic curve (ROC) to predict 1-year overall survival (OS). Based on this cut-off value (-0.258), PLC patients were categorized into high and low-immune risk groups. The survival curve was generated using the Kaplan-Meier method, and the significance of the IRGP prognostic model, along with other clinical characteristics, was assessed through univariate and multivariate Cox's proportional hazards regression models. During the univariate and multivariate Cox analysis, risk scores were obtained for clinical factors, pathological factors, and IRGPI in each dataset. The expression data of selected key IRGs were merged with survival data using R 4.1.0 and Perl 5.32.1. The merged data underwent univariate Cox regression analysis, and candidate genes meeting a significance threshold ($P < 0.05$) were identified. Subsequently, high-dimensional data were processed using LASSO regression with the "glmnet" package to obtain hub IRGs highly correlated with liver cancer prognosis [21].

2.1.4. Prediction of immune cell infiltration in PLC-related IRG expression profile

The acquired PLC-related IRG expression profile, as described in section 1.2.2, underwent immune cell infiltration prediction using the CIBERSORT platform. CIBERSORT employs vector regression to estimate the abundance of various types of immune cells within extensive tumor IRG expression profiles [22]. The analysis conducted on the CIBERSORT platform unveiled the relative proportions of 22 types of infiltrative immune cells for each sample. To calculate the relative proportions of infiltrative immune cells for each sample, the R package "CIBERSORT R script" (V1.03) was utilized. A P -value < 0.05 was statistically significant.

2.2. Validation of PLC-related hub IRGs and infiltrative immune cells

2.2.1. Validation of PLC-related hub IRGs

The risk score for hub IRGs, obtained through the IRGP prognostic model, was used to categorize patients into high and low-immune risk groups based on median gene expression. The correlation between hub IRGs and survival rate was explored using the Kaplan-Meier method, and the log-rank test computed P values between survival curves. The accuracy of the model was assessed by plotting the ROC curve. A survival curve for selected IRGs was generated using the Kaplan-Meier online tool, and protein expression levels were validated using data from the Human Protein Atlas (HPA).

2.2.2. Validation of immune cell infiltration in PLC-related IRG expression profile

Specific pathogen-free (SPF)-grade male BALB/c mice (7 weeks old, weight 20 g) were procured from Beijing SpaiFu Biotechnology Co. Ltd (SCXK (Beijing) 2019-0010) and housed in SPF conditions with regular indoor UV radiation. The H22 liver cancer cell line, adjusted to a concentration of 1×10^7 /ml, was intraperitoneally injected into mice. Cells collected in passage 3 were inoculated with 0.1 ml of the cell suspension in the right axilla. Successful modeling was confirmed 6–8 days later with palpable indurations (3–7 mm in diameter). Twenty mice were randomly assigned to two groups: the control group (NC, 0.1 ml/10 g normal saline gavage) and the model group (Model, 0.1 ml/10 g normal saline gavage). The intervention was maintained for 13 days, during which the general condition and body weight of the mice were observed and recorded every 3 days. Twenty-four hours after the last administration, mice were anesthetized using pentobarbital sodium (0.2 ml/mouse) and sacrificed following retro-orbital blood collection. Spleen and thymus tissue were isolated to calculate the viscera index [23]. Pathological changes in thymus and spleen tissues were observed to assess immune functions, and the number of relevant immune cells in blood and spleen tissue was determined. The following methods were employed for flow cytometry: Cell suspension samples were prepared using fresh blood and spleen tissue. Samples were stained with FITC-conjugated anti-CD11b and PE-conjugated anti-GR-1 at room temperature for 30 min. The percentage of CD11b/Gr-1 double-positive cells in total cells was determined to quantify the percentage of neutrophils (CD11b/GR-1). Additionally, samples were stained with APC-conjugated anti-F4/80, FITC-conjugated anti-CD11b, PE-conjugated anti-CD86, and BV421-conjugated anti-CD163 at room temperature for 30 min. The percentage of tumor-associated macrophages (TAMs) was quantified based on the percentage of CD86 and CD163 cells in F4/80 and CD11b double-positive cells (M1:F4/80, CD11b, CD86; M2:F4/80, CD11b, CD163). Subsequently, FITC-conjugated anti-CD3, APC-conjugated anti-CD4, and PE-conjugated anti-CD8 were applied for staining at room temperature for 30 min. The percentage of CD4⁺ and CD8⁺ T cells was confirmed by measuring their proportions in total T cells (CD3⁺ cells). FITC-conjugated anti-CD19, PE-conjugated anti-CD24, APC-conjugated anti-CD45R, and BV421-conjugated anti-CD138 were applied for staining at room temperature for 30 min. The proportion of B cells (CD24/CD45R) was determined by measuring the percentage of CD24 and CD45R double-positive cells in total CD19 cells. The proportion of plasma cells (CD138) was determined by measuring its percentage in total CD19 cells. All data from flow cytometry were analyzed using FlowJo-v10.6.2, and Prism software was used for figure generation. A P -value < 0.05 was statistically significant.

2.3. Statistical analysis

All statistical analyses were performed using R software. Group differences were compared using the t -test. The cumulative survival time was calculated using the Kaplan-Meier method, and differences in survival curves were analyzed using the log-rank sum test from

the “Survival” package. The “Survcomp” software package was employed to calculate the hazard ratio. Univariate and multivariate analyses were conducted using the Cox proportional hazard regression model. $P < 0.05$ was considered statistically significant. $P < 0.01$ was considered highly statistically significant.

3. Results

3.1. Prediction of PLC-related hub IRGs and infiltrative immune cells

3.1.1. Acquisition of PLC-related IRGs

A total of 544 samples, including both TCGA ($n = 377$) and GSE76427 ($n = 167$) datasets, were incorporated into the study (Table 1). The datasets were filtered using a MAD threshold of >0.5 , focusing on genes with substantial variation, which were then selected as candidate genes.

3.1.2. Model construction and definition using IRGs

The PLC transcriptome data obtained from the TCGA database and 2483 IRG (schedule 1) obtained from the ImmPort database were intersected, and 1689 TCGA immune genes were obtained (schedule 2). After the immune genes of the normal samples were removed, the intersection genes were extracted with the GEO database genes, and a total of 230 IRG were obtained (schedule 3). The obtained differential immune related genes were used to construct a prognostic model to obtain a sample IRG, and 4135 IRGPs were obtained by pairwise pairings (schedule 4). After excluding the IRGP with less variation ($MAD = 0$), the IRGPI was defined by LassoCox proportional hazard regression, and the final 84 IRGPs (schedule 5) were composed of 85 IRG. CD4|PLTP, CD8A|CXCL1, CD8A|EDNRA, CD8A|TNFRSF11B, CTSB|C8G, HLA-DOA|STC2, HLA-DQB1|PLTP, HLA-DRB1|S100A11, HLA-DRB1|S100A16, HSPA8|C8G, HSPA8|PROC, HSP90AB1|SERPIND1, ICAM1|IL1RN, MICB|LPA, and TGFBR2|CDK4. In addition, by using the LASSO regression model, we further selected 29 IRGPs as the final risk prognostic characteristics (Table 2).

3.1.3. Model validation and evaluation using IRGs

The risk score for each PLC patient from the TCGA dataset was computed using the Immune-Related Gene Pair Index (IRGPI). The optimal cut-off for IRGPI was determined to be -0.258 through time-dependent ROC curve analysis (Fig. 1a). Subsequently, PLC patients were stratified into high and low-immune risk groups based on this optimal cut-off. The high immune risk group exhibited significantly shorter OS compared to the low immune risk group ($P < 0.001$) (Fig. 1b). Univariate and multivariate Cox regression analyses were conducted to assess the predictive capability of IRGPI and its potential as an independent prognostic factor. During the univariate Cox analysis, the IRG Pair (IRGP) prognostic model risk score ($P < 0.001$, HR = 4.206, 95% CI = 3.164–5.592) and tumor T stage ($P < 0.001$, HR = 1.667, 95% CI = 1.365–2.036) were found to significantly impact prognosis. In the multivariate Cox analysis, the IRGP prognostic model risk score ($P = 0.001$, HR = 3.907, 95% CI = 2.902–5.260) and tumor T stage ($P = 0.015$, HR = 1.305, 95% CI = 1.052–1.618) were identified as independent prognostic factors ($P < 0.05$) (Fig. 1d–e). Patients in the GEO dataset were categorized into high and low-immune-risk groups using the same cut-off, and their survival rates were compared. Both groups exhibited a correlation between OS and time (Fig. 1c). During univariate Cox analysis, tumor N stage ($P = 0.004$, HR = 2.372, 95% CI = 1.310–4.294) was identified as a prognostic factor. In multivariate Cox analysis, tumor N stage ($P = 0.024$, HR = 2.437, 95% CI = 1.125–5.279) was confirmed as an independent prognostic factor ($P < 0.05$) (Fig. 1f–g). Importantly, there was heterogeneity in the correlation analysis, possibly influenced by differences in sequencing, processing, samples, and tissue.

Table 1
Patient demographics and clinical characteristics in TCGA-COAD and GSE76427 datasets.

Parameter	TCGA-COAD (n = 377)	GSE76427 (n = 167)
Age (years, $x \pm s$)	59.45 \pm 13.51	63.45 \pm 12.68
Gender [n (%)]		
Male	255 (67.64)	93 (55.69)
female	122 (32.36)	22 (13.17)
unknown	—	52 (31.14)
N Grade [n (%)]		
N0	257 (68.17)	4 (2.40)
N1	4 (1.06)	74 (44.31)
N2	115 (30.50)	28 (16.77)
unknown	1 (0.27)	61 (36.53)
T Stage [n (%)]		
T1	185 (49.07)	55 (32.93)
T2	95 (25.20)	35 (20.96)
T3	81 (21.49)	21 (12.57)
T4	13 (3.45)	3 (1.80)
unknown	3 (0.80)	53 (31.74)
Fustat [n (%)]		
alive	249 (66.05)	92 (55.09)
death	128 (33.95)	23 (13.77)
unknown	—	52 (31.14)

Table 2
The results of 29 IRGPs using LASSO regression model.

Gene	Coef	HR	HR.95L	HR.95H	coxPvalue
CD8A EDNRA	-0.120010	0.528369	0.367077	0.760531	0.000596921
CD8A TNFRSF11B	-0.279210	0.442181	0.302998	0.645299	2.32367E-05
CD8A TNFSF13B	-0.055349	0.484190	0.333072	0.703872	0.000144904
CTSB C8G	0.133971	2.062913	1.425176	2.986025	0.000124228
HLA-DQB1 PLTP	-0.171794	0.537439	0.377619	0.764900	0.000564041
HLA-DRB1 S100A16	-0.235219	0.472084	0.325867	0.683910	7.22069E-05
HSPA8 PROC	0.232923	2.177401	1.463067	3.240504	0.000125147
LGMN TMPRSS6	0.064309	2.075427	1.447433	2.975889	7.15307E-05
CXCL1 TRIM22	0.045161	2.238242	1.573609	3.183590	7.39151E-06
CXCL1 CD48	0.104362	2.022048	1.412153	2.895352	0.000120972
FABP5 CD48	0.167517	2.190554	1.436913	3.339470	0.000267457
IFIH1 BMP2	-0.235599	0.502622	0.353154	0.715351	0.000133324
TNFAIP3 RORC	0.150937	1.969727	1.348552	2.877030	0.000453299
ITGAV PIK3R1	0.341582	2.701539	1.873227	3.896118	1.03939E-07
ITGAV IL4R	0.230698	2.143645	1.492918	3.078008	3.61211E-05
CACYBP ENG	0.263725	2.248599	1.569954	3.220603	9.8397E-06
TMPRSS6 NDRG1	-0.037238	0.395314	0.273815	0.570726	7.29628E-07
IL7R SYK	-0.000963	0.427726	0.278940	0.655874	9.8689E-05
IL7R STC1	-0.108152	0.363718	0.208413	0.634753	0.000371242
IL7R TNFSF13B	-0.130982	0.487649	0.328730	0.723395	0.000358005
IL7R ICAM2	-0.149798	0.460375	0.290115	0.730556	0.00099291
CCL21 TNFRSF11B	-0.070499	0.473608	0.322344	0.695856	0.000140609
FGR TEK	0.021137	2.035058	1.403416	2.950986	0.000178656
CD79B STC2	-0.174205	0.491422	0.345849	0.698269	7.3791E-05
STC1 FYN	0.209711	2.113959	1.470204	3.039594	5.34615E-05
TGFB3 TEK	0.042380	2.334150	1.470039	3.706196	0.000326608
TNFSF13B TEK	0.058659	1.914298	1.337421	2.740002	0.000386672
RORC NCK2	-0.083779	0.439466	0.299897	0.643987	2.47353E-05
TGFBR2 CDK4	-0.243139	0.479405	0.337112	0.681760	4.27335E-05

Abbreviations: Coef, LASSO analysis coefficient; HR, risk ratio (HR > 1, indicating high-risk immune gene pair, HR < 1, indicating low-risk immune gene pair); HR.95L, the lower 95% confidence interval; HR.95H, the lower 95% confidence interval.

3.1.4. Prediction of PLC-related hub IRGs

In the prediction of PLC-related hub IRGs, we initially identified 19 candidate genes through univariate Cox regression analysis, utilizing a significance threshold of $P < 0.05$ for 85 IRGs (Fig. 2a). To identify genes with robust predictive capabilities, we employed the LASSO Cox regression model in R 4.1.0, determining the optimal λ when the median residual sum of squares was minimized. This process resulted in the selection of 11 robust genes (Fig. 2b–c) as liver cancer-related prognostic factors, including *CDK4*, *FABP5*, *NDRG1*, *FYN*, *HSPA8*, *ITGAV*, *S100A16*, *SORT1*, *STC2*, *TEK*, and *TNFRSF11B*. Further analysis involved categorizing patients into high and low-immune risk groups based on the median expression levels of the 11 candidate genes, followed by generating a survival curve (refer to Fig. 2d). The outcomes revealed that individuals in the low immune risk group exhibited longer OS compared to their counterparts in the high immune risk group. The Receiver Operating Characteristic (ROC) curve, with an area under the curve of 80.5% (Fig. 2e), underscored the prognostic potential of these 11 IRGs in liver cancer. Consequently, these genes stand out as valuable prognostic biomarkers for liver cancer.

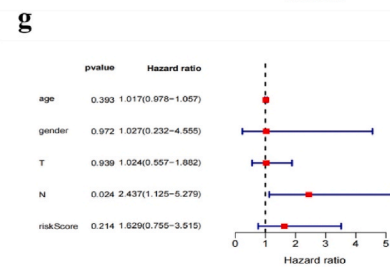
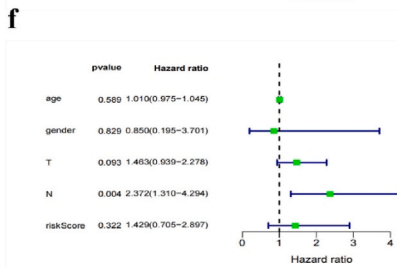
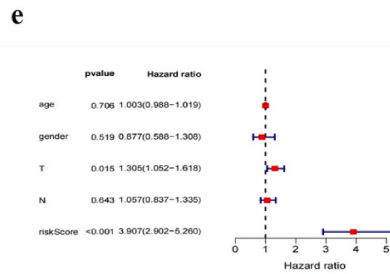
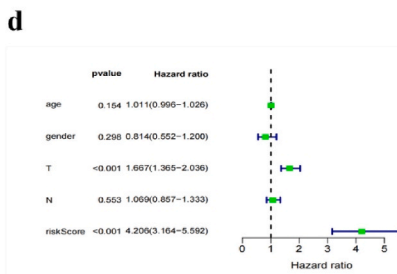
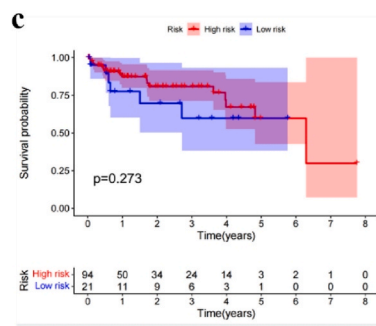
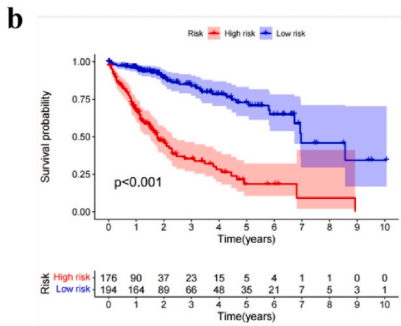
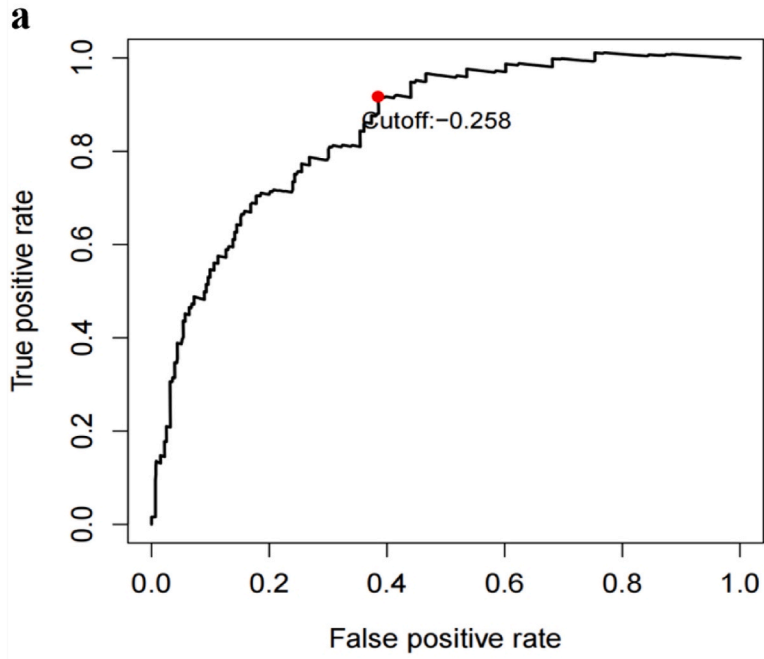
3.1.5. Analysis and prediction of PLC-related immune cell infiltration

The relative proportions and abundance of 22 kinds of immune cells in different risk groups were estimated using CiberSort (Fig. 3a). Notably, the expression profiles of infiltrated immune cells exhibited significant differences between these groups. Specifically, the high immune risk group demonstrated significantly higher expressions of neutrophils ($P = 7.442e-04$), M0 macrophage ($P = 3.071e-16$), and M2 macrophage ($P = 0.013$). In contrast, the low immune risk group exhibited elevated expression levels of M1 macrophage ($P = 0.003$), naive B cells ($P = 2.073e-06$), plasma cells ($P = 0.008$), $CD4^+$ memory T cells ($P = 0.039$), and $CD8^+$ T cells ($P = 2.201e-10$) (Fig. 3b–i).

3.2. Validation of PLC-related hub IRGs and infiltrative immune cells

3.2.1. Validation of PLC-related hub IRGs

Survival curves were plotted using Kaplan-Meier estimates (Fig. 4a–k), and HR of PLC-related hub IRGs were calculated using the Cox regression model. The results demonstrated that the high expression group, characterized by elevated levels of *FYN*, *HSPA8*, *ITGAV*, *S100A16*, *SORT1*, *STC2*, *TEK*, and *TNFRSF11B*, exhibited a lower survival rate compared to the low expression group. Conversely, the high expression group, featuring *CDK4*, *FABP5*, and *NDRG1*, displayed a higher survival rate than the low expression group. These findings provide compelling evidence of a close correlation between the expression patterns of these 11 genes and the survival outcomes of PLC patients, with statistical significance set at $P < 0.05$. To further validate the transcript levels of these 11 genes, we utilized data from HPA. The analysis revealed that the transcript levels of *NDRG1*, *FYN*, *HSPA8*, and *SORT1* in liver cancer



(caption on next page)

Fig. 1. Validation and evaluation of the prognostic model using IRGs. (a) ROC curve of IRGPI variation over time in the TCGA dataset. (b) Kaplan-Meier curve of OS of patients from the high and low immune risk groups in the TCGA dataset. (c) Kaplan-Meier curve of OS of patients from the high and low immune risk groups in the GEO dataset. (d–e) Forest plot of univariate and multivariate Cox analyses for prognostic factors in the TCGA dataset. (f–g) Forest plot of univariate and multivariate Cox analyses for prognostic factors in the TCGA dataset.

tissue were higher than in normal liver tissue. Conversely, *CDK4*, *FABP5*, *S100A16*, and *TEK* showed no significant difference between liver cancer and normal tissue (Fig. 5).

3.2.2. Analysis and validation of immune cell infiltration in PLC-related IRG expression profile

To assess and validate immune cell infiltration in the context of PLC-related IRG expression profiles, an H22 liver cancer tumor-bearing mouse model was established. Experimental results revealed that the Model group exhibited significantly reduced body weight, spleen index, and thymus index compared to the Normal group (all $P < 0.001$) (Fig. 6a–c). Histopathological examination via Hematoxylin and Eosin (HE) staining provided insights into the structural changes. In the Normal group, mice displayed intact thymus tissue membranes, clear corticomedullary demarcation, a thick cortex with dense lymphocytes, and a small, lightly colored medullary region containing abundant thymic epithelial cells and lymphocytes. Conversely, the Model group exhibited alterations such as thinned cortex, reduced lymphocytes with loosely arranged cells, an enlarged medullary region with light coloring, and spherical or polygonal thymic epithelial cells with large cell bodies (Fig. 6d). Furthermore, HE staining of spleen tissues indicated that the normal group had intact membranes without hyperplasia, a clear border between the white pulp and red pulp, and no atrophy in the white pulp. In contrast, the Model group displayed significantly thickened membranes, a clear border between red and white pulps, partial atrophy in the white pulp with reduced area, extramedullary hematopoiesis in the red pulp, and local aggregation of erythroid lineages (Fig. 6e). Flow cytometry (FACS) analysis highlighted the immune alterations induced by liver cancer xenograft. The Model group exhibited elevated proportions of neutrophils, M2/M1 ratio, and $CD4^+/CD8^+$ ratio, along with reduced percentages of naive B cells and plasma cells in peripheral blood and spleen tissue compared to the Normal group (all $P < 0.0001$) (Fig. 7a1–e2). Collectively, these findings underscore the profound impact of liver cancer xenografts on the immune function of mice.

4. Discussion

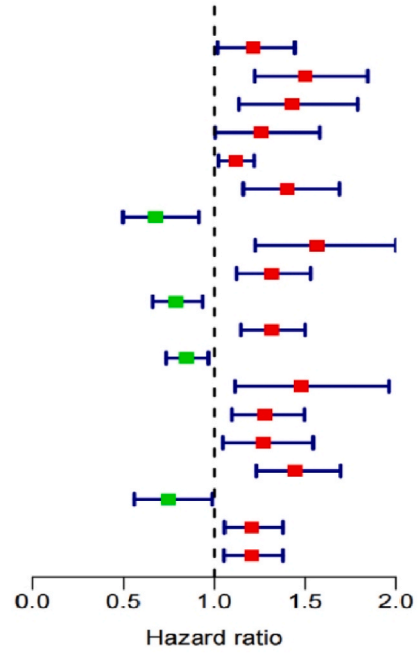
PLC is a prevalent malignancy of the digestive system, characterized by its insidious symptom onset, delayed diagnosis, tendency for postoperative recurrence, and overall poor prognosis. The current focus on cancer cells in PLC diagnosis, therapeutic decisions, and prognosis evaluation centers around early detection of alpha-fetoprotein (AFP). However, the fact that 32–59% of liver cancer patients exhibit normal AFP levels suggests that AFP is neither a standard diagnostic criterion nor the optimal measure for assessing cancer prognosis and survival [2]. Biomarkers identified in both domestic and international studies have significantly contributed to enhancing the diagnosis and treatment of PLC, addressing its challenging prognosis and high recurrence rate [24,25]. Nevertheless, there is an urgent need for robust prognostic biomarkers to predict the survival of PLC patients, considering factors such as biological complexity, individual differences, and immunological aspects. With this imperative in mind, we have employed bioinformatics methodologies, leveraging clinical data from tumor databases, to identify reliable prognostic biomarkers. This strategic approach not only aims to uncover new therapeutic targets for liver cancer treatment but also seeks to tailor measures for PLC patients based on a more comprehensive understanding of the disease.

First, we sourced liver cancer datasets from TCGA and GEO databases, specifically the TCGA dataset with a sample size of 377 and the GEO GSE76427 dataset with a sample size of 167. Through a rigorous screening process of these datasets, we intersected the acquired genes with 2483 IRGs from the ImmPort database, resulting in the identification of 1689 differentially expressed IRGs. Pairing these genes allowed us to derive IRGPs, and those with minimal variation ($MAD = 0$) were excluded from further consideration. Subsequently, the IRGPI was defined using Lasso Cox proportional hazards regression, leading to the identification of 84 significant IRGPs. Notably, these 84 IRGPs, along with 85 individual IRGs, collectively constituted a comprehensive prognostic risk model. The successful establishment of this model enabled the categorization of patients into high and low-immune risk groups using an optimal cut-off. Notably, the high immune risk group exhibited a significantly shorter OS compared to the low immune risk group ($P < 0.001$), underscoring the pivotal role of IRGPI as a critical prognostic factor for PLC. To further elucidate the implications of IRGPI on additional clinical factors, univariate and multivariate Cox regression analyses were conducted using the TCGA dataset. These analyses revealed that the IRGPI model risk score, along with the tumor T stage, emerged as independent prognostic factors for PLC patients.

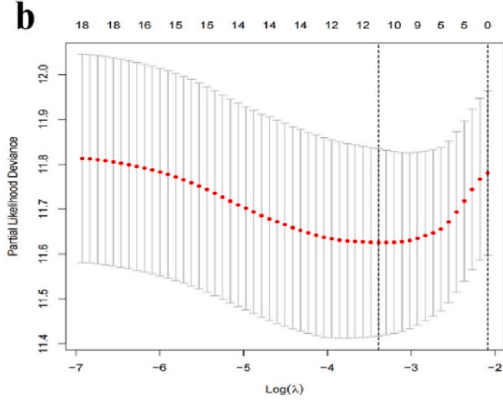
Nineteen candidate genes were identified through univariate Cox regression analysis of 85 IRGs using R version 4.1.0 and Perl version 5.32.1, with a significance threshold of $P < 0.05$. Subsequently, a LASSO Cox regression model was constructed to refine the selection, resulting in the identification of 11 genes with optimal predictive performance, determined by the median residual sum of squares ($\lambda = 11$). The final set of 11 genes comprised *CDK4*, *FABP5*, *NDRG1*, *FYN*, *HSPA8*, *ITGAV*, *S100A16*, *SORT1*, *STC2*, *TEK*, and *TNFRSF11B*. Analysis of survival rates revealed that the group exhibiting high expression levels of *FYN*, *HSPA8*, *ITGAV*, *S100A16*, *SORT1*, *STC2*, *TEK*, and *TNFRSF11B* exhibited lower survival rates compared to the low expression group. Conversely, the group with elevated expression of *CDK4*, *FABP5*, and *NDRG1* displayed higher survival rates than the low-expression group. Validation of transcript expression levels was conducted using HPA data. Notably, the transcript expression levels of *NDRG1*, *FYN*, *HSPA8*, and *SORT1* in liver cancer tissue were higher than those in normal liver tissue. Meanwhile, the transcript expression levels of *ITGAV*, *STC2*, and *TNFRSF11B* in liver cancer were lower than in normal tissue. However, no significant differentiation was observed between liver

a

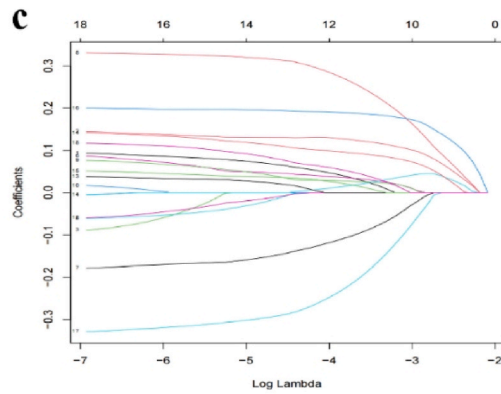
	pvalue	Hazard ratio
BMP2	0.031	1.212(1.018–1.443)
CDK4	<0.001	1.501(1.223–1.844)
CMTM7	0.002	1.425(1.136–1.789)
CTSB	0.046	1.259(1.004–1.580)
CXCL1	0.014	1.117(1.023–1.220)
FABP5	<0.001	1.399(1.159–1.689)
FYN	0.011	0.674(0.497–0.914)
HSPA8	<0.001	1.566(1.226–2.000)
ITGAV	<0.001	1.312(1.123–1.532)
LPA	0.007	0.787(0.662–0.936)
NDRG1	<0.001	1.312(1.148–1.500)
NR1H2	0.015	0.843(0.735–0.967)
PSMD10	0.007	1.478(1.114–1.961)
S100A16	0.002	1.281(1.096–1.496)
SORT1	0.015	1.272(1.048–1.544)
STC2	<0.001	1.445(1.232–1.696)
TEK	0.041	0.744(0.560–0.987)
TNFRSF11B	0.006	1.206(1.056–1.377)
TNFRSF21	0.006	1.205(1.054–1.377)



b

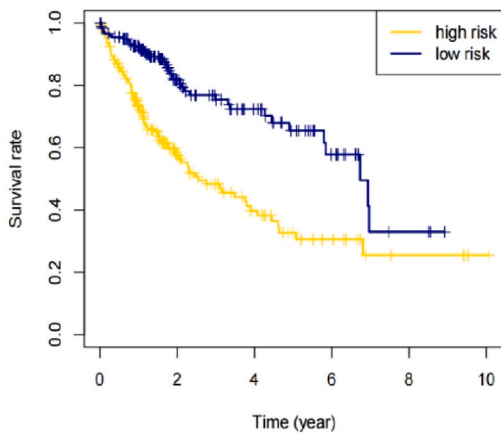


c



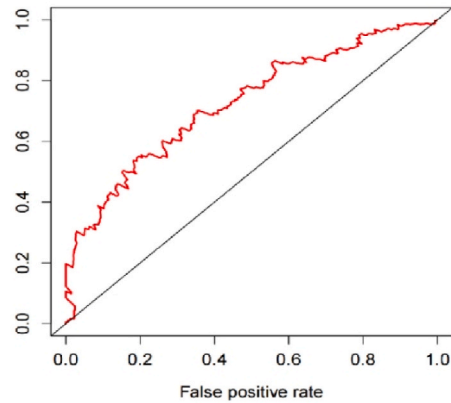
d

Survival curve (p=1.824e-07)



e

ROC curve (AUC = 0.805)



(caption on next page)

Fig. 2. PLC-related hub IRG selection and survival analysis. (a) Forest plot of hazard ratios (HRs) of 85 liver cancer-related IRGs. (b) Partial likelihood deviance and λ were plotted using the LASSO Cox regression models. (c) Selected variable coefficients were expressed as lambda parameters. (d) Kaplan-Meier survival plots of the two groups. (e) ROC curve (AUC = 80.5%).

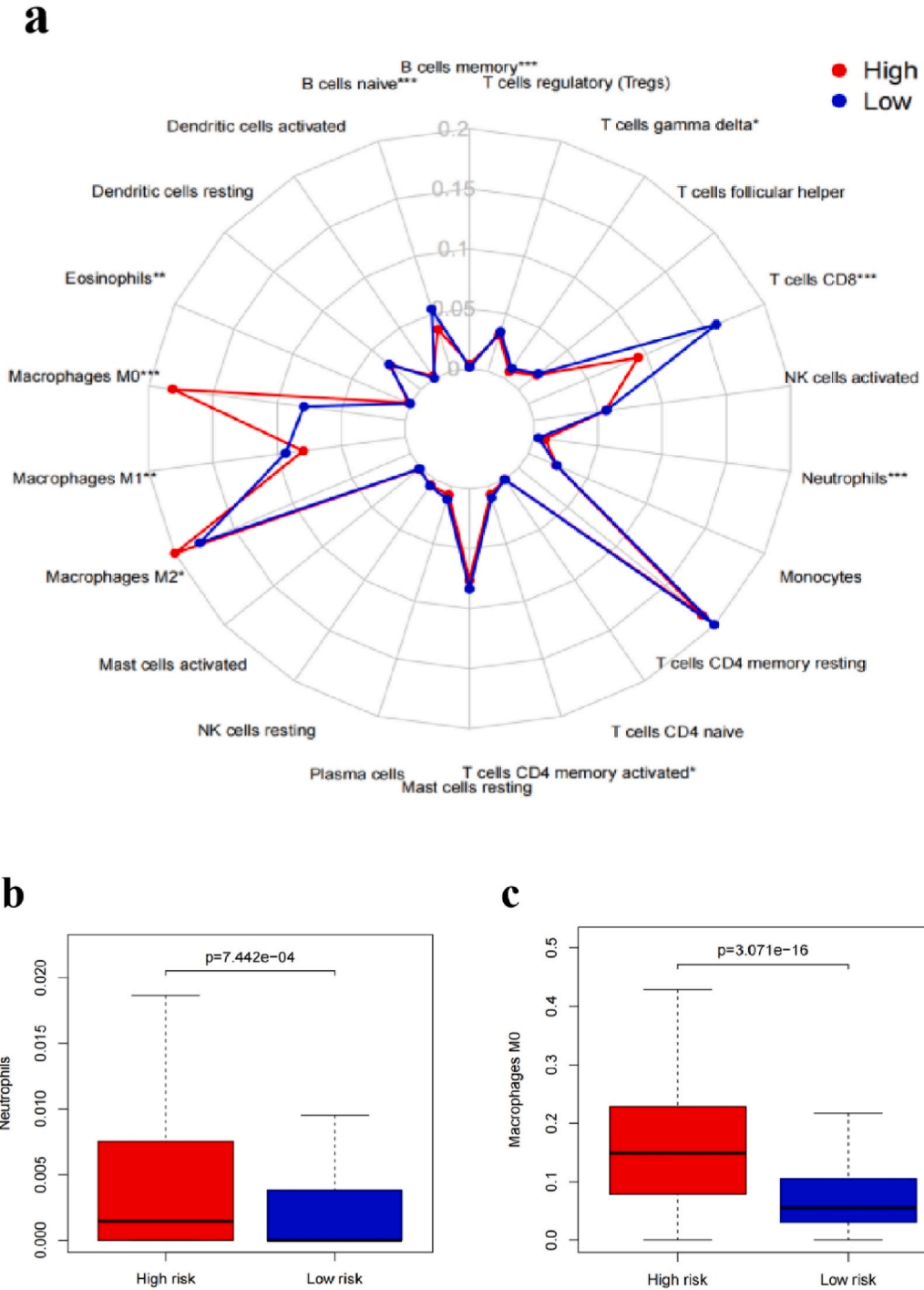


Fig. 3. Analysis and prediction of PLC-related immune cell infiltration. (a) CIBERSORT estimating the abundance of the 22 kinds of immune cells in the high and low-immune-risk groups. (b-i) Abundance distribution of specific immune cells in the high and low immune risk groups.

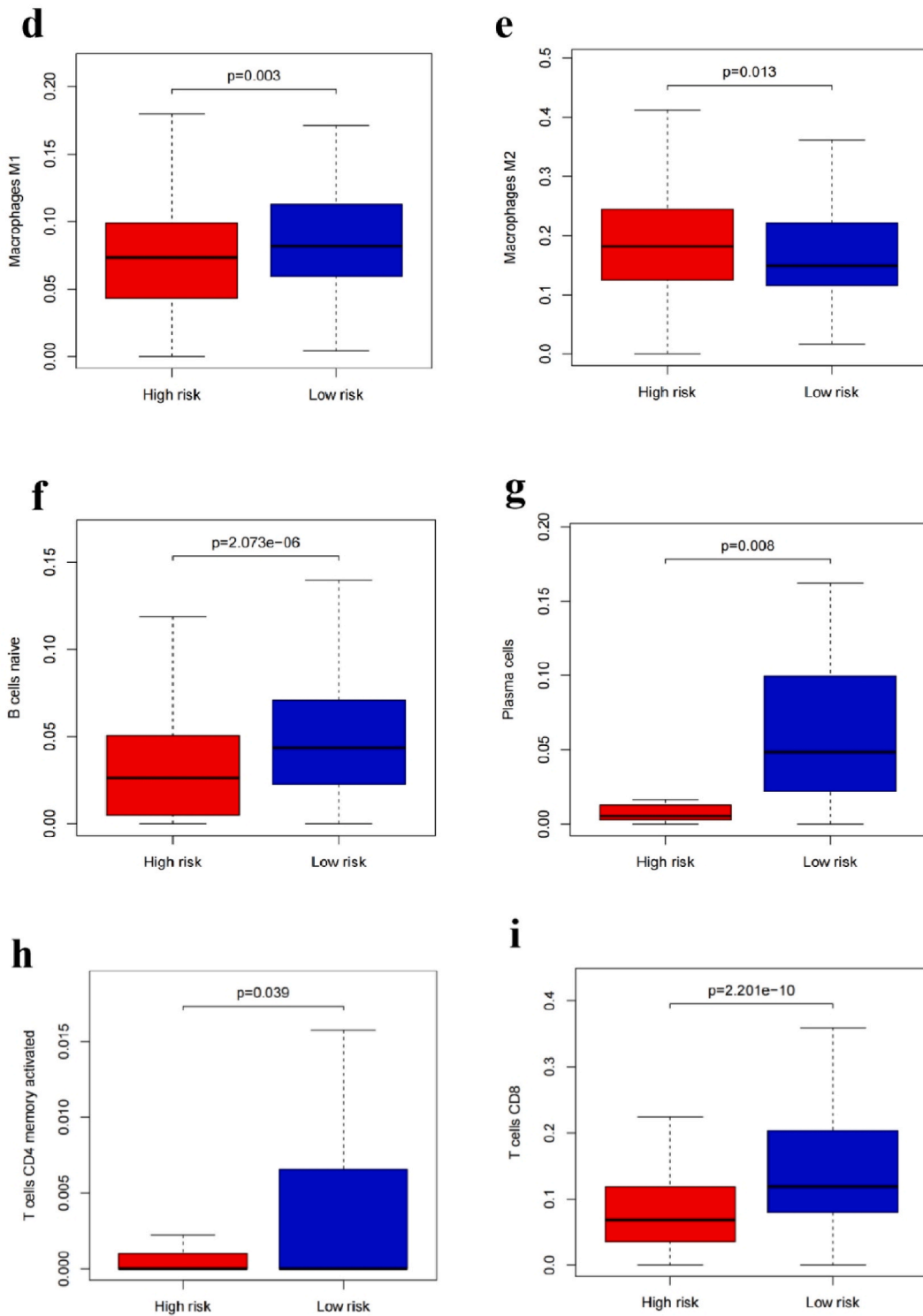


Fig. 3. (continued).

cancer and normal liver tissue for *CDK4*, *FABP5*, *S100A16*, and *TEK*. This lack of differentiation may be attributed to inherent biological heterogeneity in tumors and potential technical biases across different sequencing platforms. Extensive research has substantiated that the 11 hub IRGs serve as prognostic biomarkers across multiple cancers [26]. *CDK4* exhibits heightened expression in human osteosarcoma cells and tissues, promoting cell proliferation and metastasis, and correlates with unfavorable prognosis in

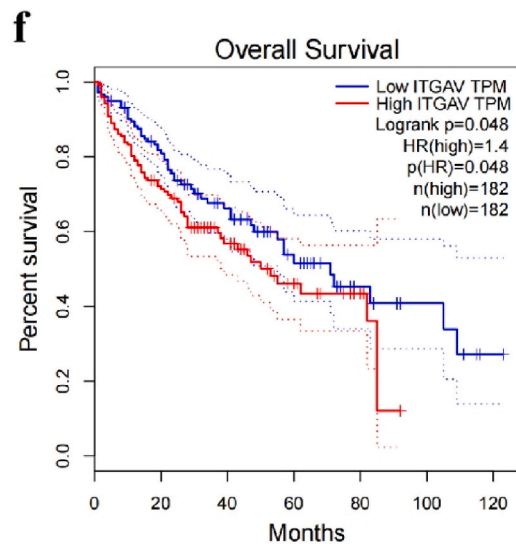
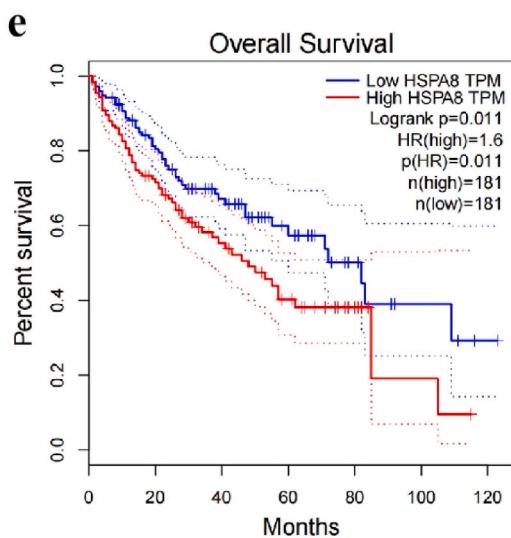
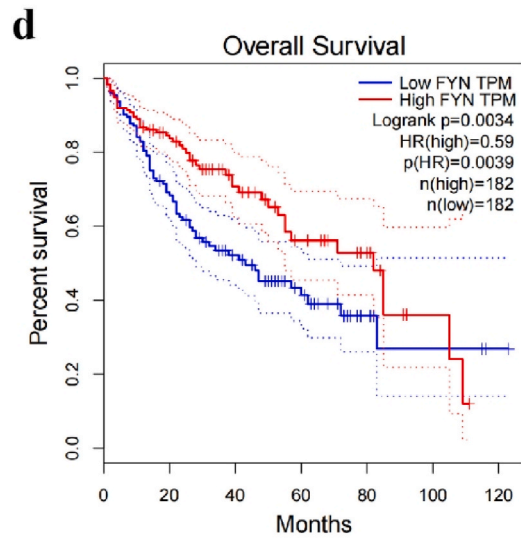
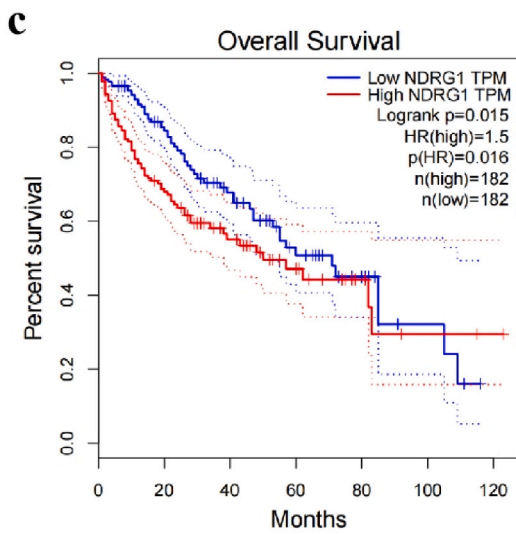
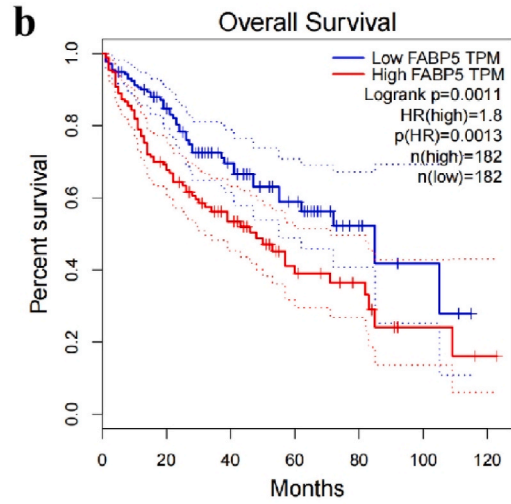
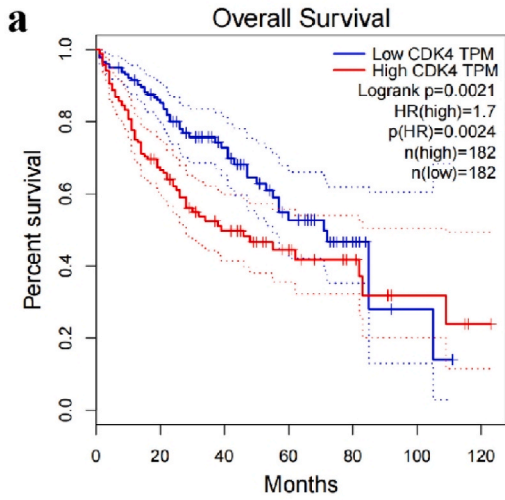


Fig. 4. Survival analysis of 11 IGRs. (a) CDK4; (b) FABP5; (c) NDRG1; (d) FYN; (e) HSPA8; (f) ITGAV; (g) S100A16; (h) SORT1; (i) STC2; (j) TEK; (k) TNFRSF11B.

osteosarcoma patients [27]. *FABP5*, overexpressed in human liver cancer cells, contributes to abnormal lipid metabolism and immune cell CD137⁺ Tex infiltration, thereby facilitating hepatocellular carcinoma (HCC) initiation and progression. *FABP5* emerges as a potential prognostic biomarker for HCC [28]. Additionally, *FABP5* demonstrates upregulated expression in cervical cancer, positively correlating with lymph node metastasis and serving as an independent prognostic predictor for cervical cancer with lymph node metastasis [29]. *NDRG1* exhibits dual effects in various cancers, displaying both pro-cancer and anti-cancer properties. In invasive breast cancer, high *NDRG1* expression is closely linked to poor survival rates, driving tumor development and brain metastasis. *NDRG1* thus presents itself as a therapeutic target and prognostic biomarker for invasive breast cancer [30,31]. *FYN* overexpression promotes migration and invasiveness in gastric cancer cells, positively correlating with gastric cancer metastasis, positioning it as a potential therapeutic target for gastric cancer [32,33]. *HSPA8*, a member of the HSP70 family, is highly expressed in cancer cells and is intricately associated with cell growth, apoptosis, and autophagy. Downregulation of *HSPA8* in pancreatic cancer inhibits cancer cell growth by affecting autophagy, making it a potential target for pancreatic cancer treatment [34]. *ITGAV*, highly expressed in breast cancer cells, influences cell proliferation, metastasis, invasion, and self-renewal. Silencing *ITGAV* expression suppresses these processes, hindering tumor growth [35]. *S100A16* overexpression in gastric cancer advances cell proliferation and migration, correlating with poor prognosis in gastric cancer patients [36]. High *SORT1* expression has been associated with advanced gastric cancer and indicates a poor prognosis [37]. *SORT1* overexpression also stimulates colorectal cancer cell growth and migration to promote tumor growth, suggesting it is a potential biomarker for the diagnosis and prognosis of colorectal cancer [38]. Downregulation of *TEK* expression promotes the proliferation and migration of clear cell renal cell carcinoma (ccRCC) cells, activating AKT phosphorylation to suppress apoptosis and tumor growth. *TEK* stands out as a potential biomarker for ccRCC [39]. *TNFRSF11B*, highly expressed in the gastric cancer cell cytoplasm, significantly enhances cell proliferation, migration, and invasion in vitro, demonstrating tumorigenic ability both in vitro and *in vivo* [40]. This comprehensive validation aligns with the initial prediction that PLC-related IGRs play pivotal roles in the initiation, development, and prognosis of diverse cancers. Furthermore, analysis based on the prognostic model and validation using clinical samples underscores the potential of PLC-related hub IGRs as valuable biomarkers for both the treatment and diagnosis of PLC.

Liver cancer, characterized by high incidence, frequent recurrence, and low survival rates, is predominantly managed through surgical intervention and comprehensive multidisciplinary therapy. Historically, immunotherapy has played a limited role in liver cancer treatment. However, its potential to elicit tumor-specific immunity by reinforcing immune responses, identifying and eliminating tumor cells, and preventing recurrence through the activation of immune pathways has garnered increased attention in recent years. Immunotherapeutic approaches, such as immune checkpoint inhibitors (e.g., CTLA-4, PD-1, PD-L1) and small molecule immunotherapy, have shown promise in improving the prognosis of HCC patients [41–43]. Tumor immunotherapy is intricately linked to the infiltration of immune cells in the tumor microenvironment, including myeloid-derived suppressor cells (MDSCs), TAMs, and other immune components that influence tumor cell proliferation, invasion, and metastasis [44]. In this study, the differential expression levels of 22 immune cell types in distinct risk groups were estimated using CIBERSORT. The analysis revealed significantly elevated expression of neutrophils, M0 macrophage, and M2 macrophage in the high immune risk group, while M1 macrophages, naive B cells, plasma cells, CD4⁺ memory T cells, and CD8⁺ T cells exhibited higher expression in the low immune risk group. Existing research supports the notion that the increased presence of neutrophils, M0 macrophages, and M2 macrophages in the tumor microenvironment leads to continuous variations in tumors and disrupts the tumor microenvironment, suppressing antitumor immune responses [45,46]. Conversely, low expression levels of M1 macrophage, naive B cells, and plasma cells fail to protect the host against pathogens, inducing immune imbalance and host tissue damage, thereby promoting tumor development and malignant transformation [47,48]. Interestingly, another study employing multiple immunostaining methods demonstrated that HCC patients with high immune cell infiltration, particularly B cells, plasma cells, and T cells, experienced favorable prognoses [49]. CD4⁺ memory T cells and CD8⁺ T cells, integral to the overall tumor immune response, were found to be correlated with tumor prognosis [50,51]. To further validate these findings, an H22 liver cancer tumor-bearing mouse model was constructed and assessed using flow cytometry. The results indicated that mice in the Model group exhibited reduced body weight, pronounced pathological changes in the spleen and thymus, and significantly lower spleen and thymus indexes compared to the Normal group. Additionally, the Model group showed an increased percentage of neutrophils, elevated M2/M1 cell ratio, and CD4⁺/CD8⁺ cell ratio, along with a decreased percentage of naive B cells and plasma cells in peripheral blood and spleen tissue compared to the Normal group. These outcomes collectively highlight the substantial impact of liver cancer xenografts on the immune function of mice. The experimental verification in H22 tumor-bearing mice provides valuable insights into the differential alterations in PLC-related immune cells, shedding light on the intricate relationship between PLC-related immune cells and the progression and prognosis of liver cancer.

5. Conclusion

In this study, we identified 11 hub IGRs associated with PLC using data from TCGA and GEO databases. The identified genes are *CDK4*, *FABP5*, *NDRG1*, *FYN*, *HSPA8*, *ITGAV*, *S100A16*, *SORT1*, *STC2*, *TEK*, and *TNFRSF11B*. A prognostic model was meticulously constructed to assess the correlation between these PLC-related hub IGRs and the survival of individuals with PLC. Additionally, we investigated the differential expression patterns of these hub IGRs across diverse patient profiles by analyzing clinical sample data from the HPA database. Furthermore, we investigated the impact of immune cell infiltration on PLC patients with varying prognoses using both the CIBERSORT platform and experimental methods. By exploring the interplay between immune cells and PLC-related hub IGRs,

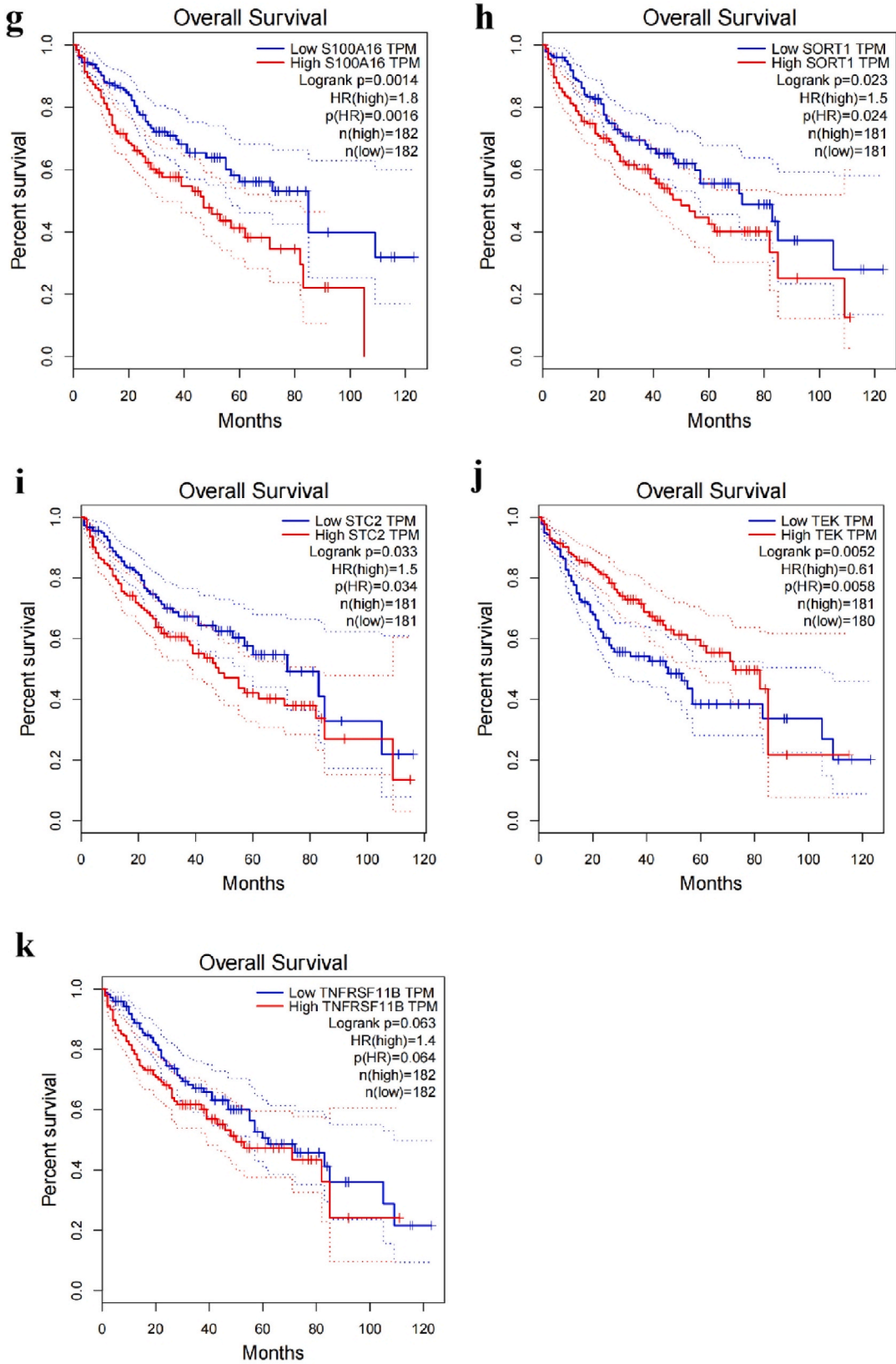


Fig. 4. (continued).

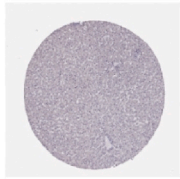
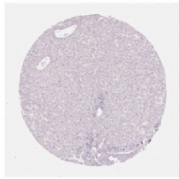
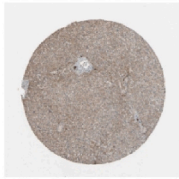
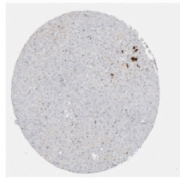
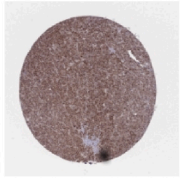
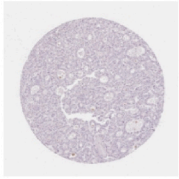
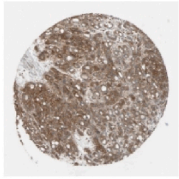
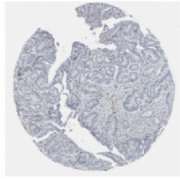
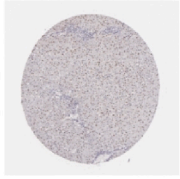
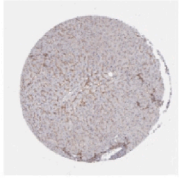
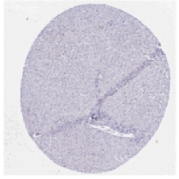
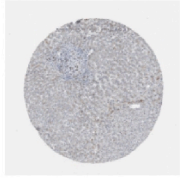
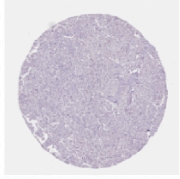
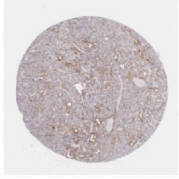
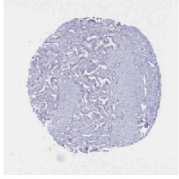
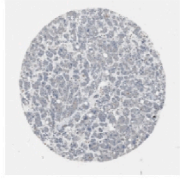
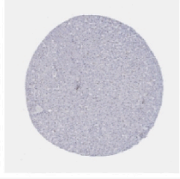

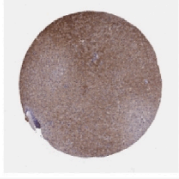
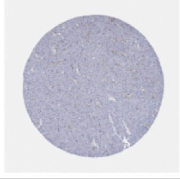
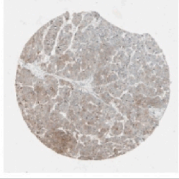
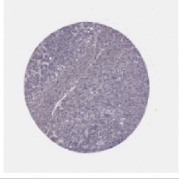
Gene	CDK4	FABP5	NDRG1	FYN
Normal				
	Not detected	Not detected	Low	Medium
Tumor				
	Not detected	Not detected	High	Not detected
Gene	HSPA8	ITGAV	S100A16	SORT1
Normal				
	Medium	Not detected	Not detected	Low
Tumor				
	Not detected	Low	Not detected	Not detected
Genes	STC2	TEK	TNFRSF11B	
Normal				
	Not detected	Low	High	
Tumor				
	Medium	Low	Low	

Fig. 5. Validation of expression levels of prognostic IRGs.

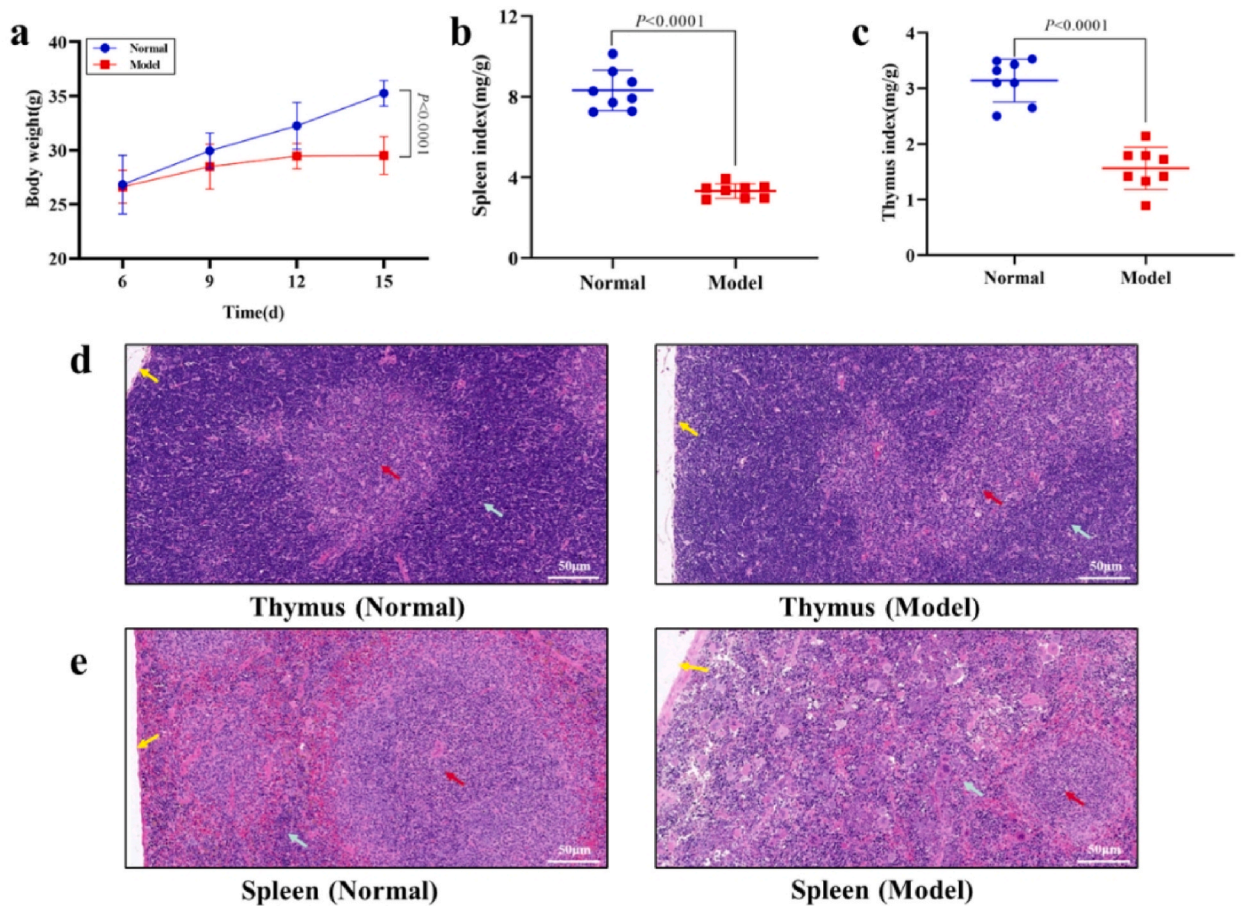


Fig. 6. Body weight variation and viscera index of liver cancer mouse model. (a) Body weight variation of H22 tumor-bearing mice. (b) Spleen index variation. (c) Thymus index variation; (d) Thymus HE staining; (e) Spleen HE staining.

we aimed to enhance our understanding of the intricate dynamics within PLC. This comprehensive analysis not only deepens our insights into the roles of PLC-related IRGs but also uncovers potential targets for immunotherapeutic interventions in the context of primary liver cancer.

Funding

This work was sponsored by the Gansu Provincial Key Research and Development Project (2015-RC-24) and the Gansu Provincial Development and Reform Commission Project (2305142201).

Ethics statement

The animal experiments in this study were approved by the Ethics Committee for Animal Experiments of Gansu University of Traditional Chinese Medicine, Ethics No. 2022-525.

Data availability

The datasets generated and/or analyzed during the current study are available from the corresponding author on reasonable request.

CRedit authorship contribution statement

Yu-Ping Yang: Writing – original draft. **Min Bai:** Writing – original draft. **Yin-Xia Cheng:** Writing – original draft. **Xin Feng:** Software, Data curation. **Yan-Ying Zhang:** Project administration. **Yuan-Yuan Zhang:** Formal analysis, Data curation. **Meng-Ya Liu:** Visualization, Formal analysis. **Yong-Qiang Duan:** Writing – original draft, Project administration.

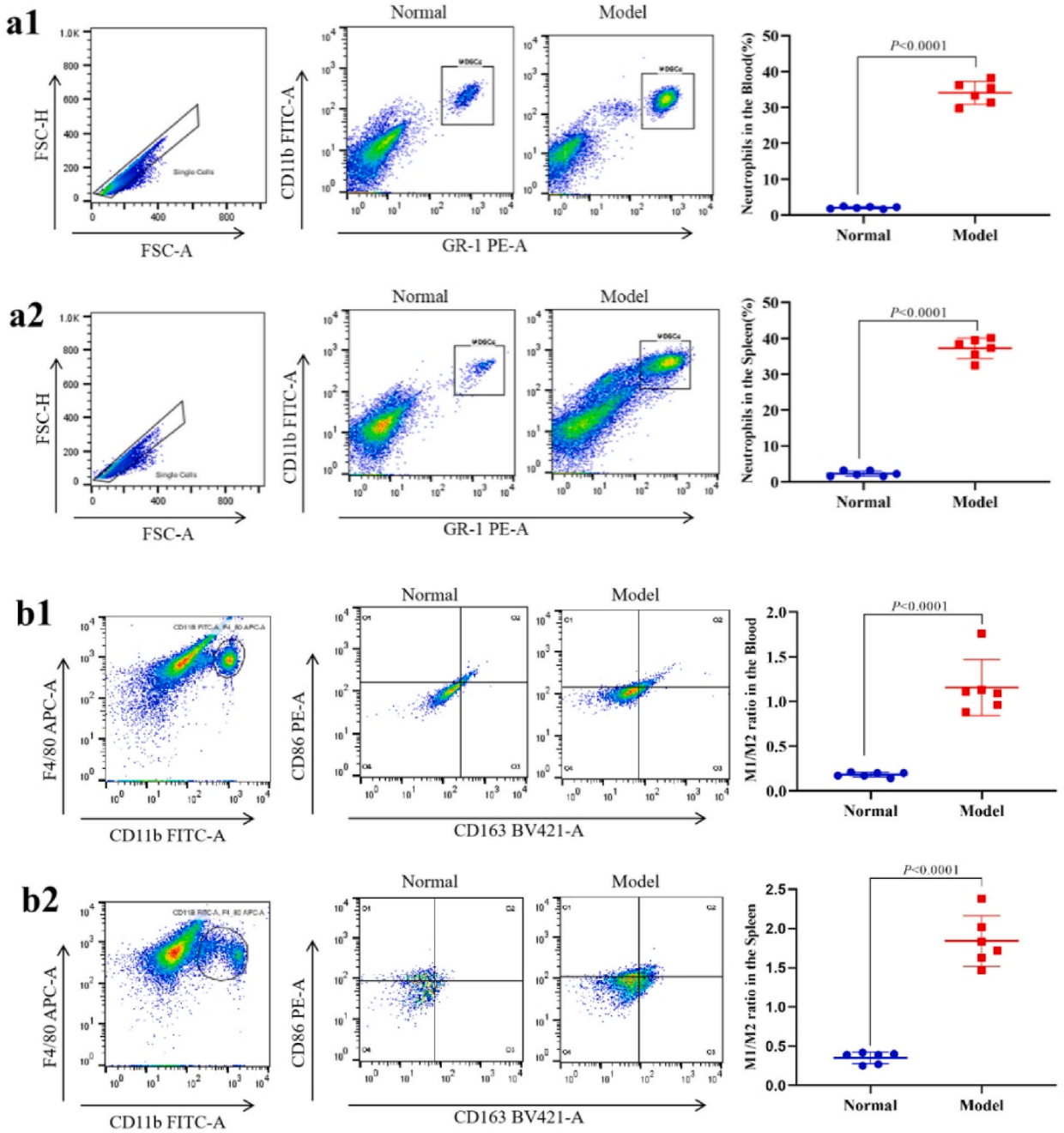


Fig. 7. Immune cell infiltration variation in the peripheral blood and liver tissue of H22 tumor-bearing mice. (a1-2) Double positivity analysis for CD11b and Gr-1 expression and diagram showing the percentage of neutrophils. (b1-2) CD163/CD86 cells were gated for F4/80 and CD11b and diagram showing M2/M1 ratio. (c1-2) CD4⁺/CD8⁺ cells were gated for CD3⁺ and diagram showing CD4⁺/CD8⁺ ratio. (d1-e1) CD24 and CD45R cells were gated for CD19 and diagram showing B cell percentage. (d2-e2) CD138 cells were gated for CD19 and diagram showing plasma cell percentage.

Declaration of competing interest

The authors declare that they have no known competing financial interests or personal relationships that could have appeared to influence the work reported in this paper.

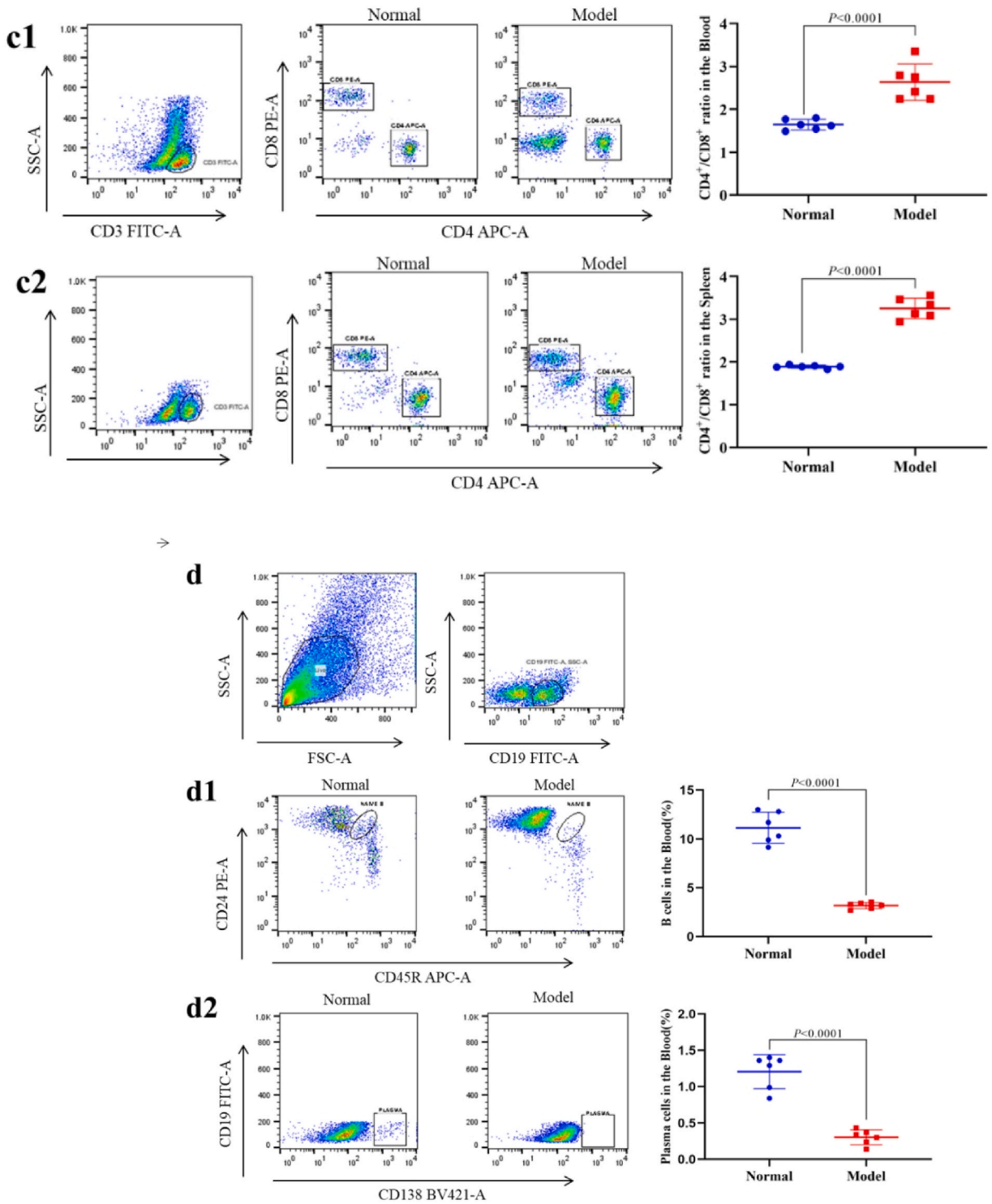


Fig. 7. (continued).

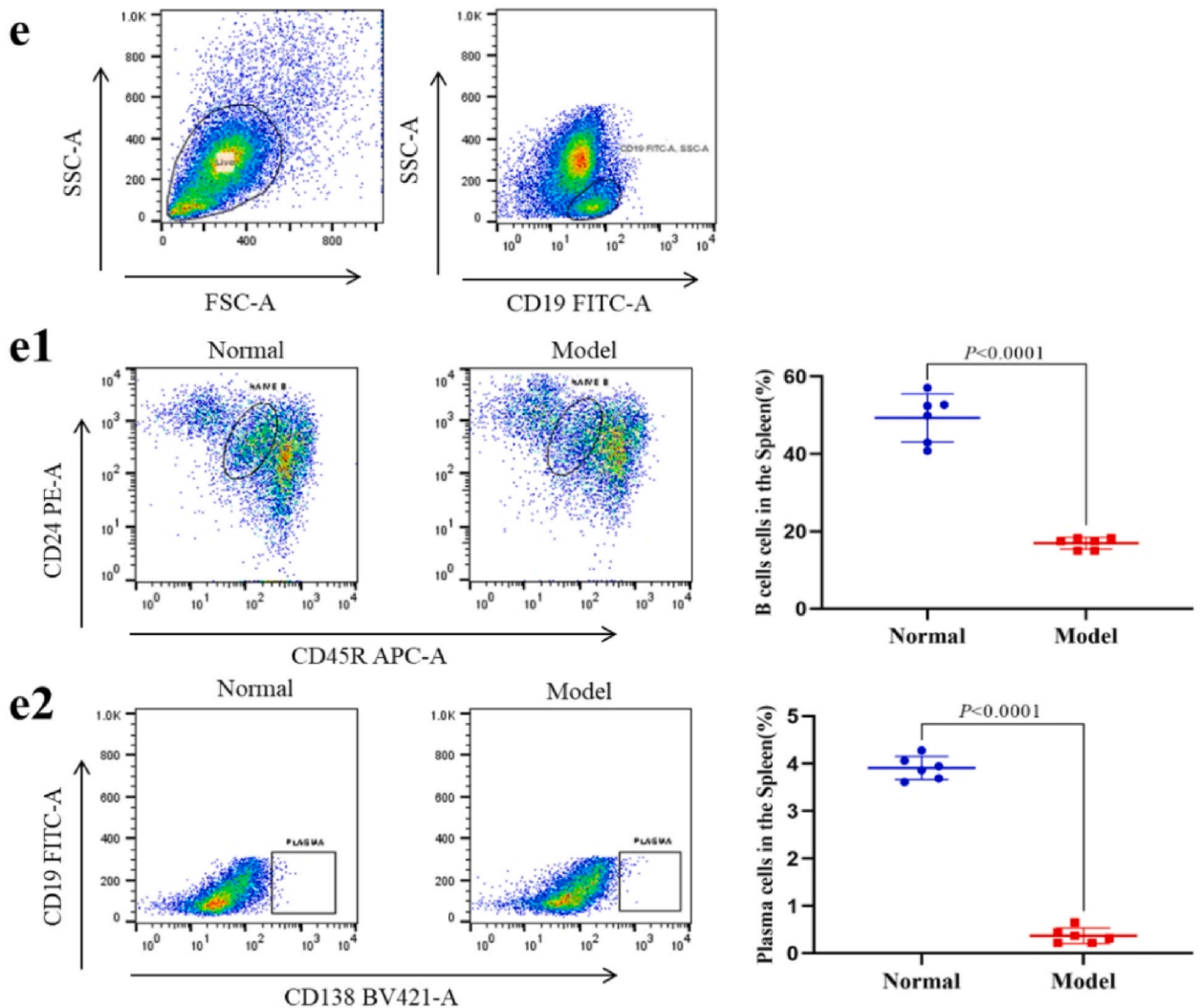


Fig. 7. (continued).

Appendix A. Supplementary data

Supplementary data to this article can be found online at <https://doi.org/10.1016/j.heliyon.2024.e27362>.

References

- [1] D. Anwanwan, S.K. Singh, S. Singh, et al., Challenges in liver cancer and possible treatment approaches, *Biochim. Biophys. Acta Rev. Canc* 1873 (1) (2020) 188314.
- [2] S. Gao, J. Gang, M. Yu, et al., Computational analysis for identification of early diagnostic biomarkers and prognostic biomarkers of liver cancer based on GEO and TCGA databases and studies on pathways and biological functions affecting the survival time of liver cancer, *BMC Cancer* 21 (1) (2021) 791.
- [3] K.A. McGlynn, J.L. Petrick, W.T. London, Global epidemiology of hepatocellular carcinoma: an emphasis on demographic and regional variability, *Clin. Liver Dis.* 19 (2015) 223–238.
- [4] L. Li, H. Wang, Heterogeneity of liver cancer and personalized therapy, *Cancer Lett.* 379 (2) (2016) 191–197.
- [5] T. Yamashita, S. Kaneko, [Liver cancer], *Rinsho Byori* 64 (7) (2016 Jul) 787–796.
- [6] K. Oura, A. Morishita, J. Tani, et al., Tumor immune microenvironment and immunosuppressive therapy in hepatocellular carcinoma: a review, *Int. J. Mol. Sci.* 22 (11) (2021) 5801.
- [7] D. Busato, et al., Novel immunotherapeutic approaches for hepatocellular carcinoma treatment, *Expert Rev. Clin. Pharmacol.* 12 (5) (2019) 453–470.
- [8] J. Bruix, S. Qin, P. Merle, et al., Regorafenib for patients with hepatocellular carcinoma who progressed on sorafenib treatment (RESORCE): a randomised, double-blind, placebo-controlled, phase 3 trial [published correction appears in *Lancet*, *Lancet* 389 (10064) (2017) 56–66, 2017 Jan 7;389(10064):36].
- [9] Z. Chen, S. Shen, B. Peng, et al., Intratumoural GM-CSF micro-spheres and CTLA-4 blockade enhance the antitumour immunity induced by thermal ablation in a subcutaneous murine hepatoma model, *Int. J. Hyperther.* 25 (2009) 374–382.

- [10] A.W. Thomson, P.A. Knolle, Antigen-presenting cell function in the tolerogenic liver environment, *Nat. Rev. Immunol.* 10 (11) (2010) 753–766.
- [11] R.L. Siegel, K.D. Miller, A. Jemal, Cancer statistics, 2020, *CA A Cancer J. Clin.* 70 (1) (2020) 7–30.
- [12] B. Zhang, X. Nie, X. Miao, et al., Development and verification of an immune-related gene pairs prognostic signature in ovarian cancer, *J. Cell Mol. Med.* 25 (6) (2021) 2918–2930.
- [13] N. Ren, B. Liang, Y. Li, Identification of prognosis-related genes in the tumor microenvironment of stomach adenocarcinoma by TCGA and GEO datasets, *Biosci. Rep.* 40 (10) (2020) BSR20200980.
- [14] D. Anwanwan, S.K. Singh, S. Singh, et al., Challenges in liver cancer and possible treatment approaches, *Biochim. Biophys. Acta Rev. Canc* 1873 (1) (2020) 188314.
- [15] J. Liu, G. Sun, S. Pan, et al., The Cancer Genome Atlas (TCGA) based m6A methylation-related genes predict prognosis in hepatocellular carcinoma, *Bioengineered* 11 (1) (2020) 759–768.
- [16] W. Cheng, X. Ren, C. Zhang, et al., Bioinformatic profiling identifies an immune-related risk signature for glioblastoma, *Neurology* 86 (24) (2016) 2226–2234.
- [17] Z. Wang, Q. Song, Z. Yang, et al., Construction of immune-related risk signature for renal papillary cell carcinoma, *Cancer Med.* 8 (1) (2019) 289–304.
- [18] S. Kobold, S. Pantelyushin, F. Rataj, et al., Rationale for combining bispecific T cell activating antibodies with checkpoint blockade for cancer therapy, *Front. Oncol.* 8 (2018) 285. Published 2018 Jul 25.
- [19] A. Popovic, E.M. Jaffee, N. Zaidi, Emerging strategies for combination checkpoint modulators in cancer immunotherapy, *J. Clin. Invest.* 128 (8) (2018) 3209–3218.
- [20] R.S. Finn, S. Qin, M. Ikeda, et al., Atezolizumab plus bevacizumab in unresectable hepatocellular carcinoma, *N. Engl. J. Med.* 382 (20) (2020) 1894–1905.
- [21] Y. Li, J. Gu, F. Xu, et al., Transcriptomic and functional network features of lung squamous cell carcinoma through integrative analysis of GEO and TCGA data, *Sci. Rep.* 8 (1) (2018) 15834. Published 2018 Oct 26.
- [22] A.M. Newman, C.L. Liu, M.R. Green, et al., Robust enumeration of cell subsets from tissue expression profiles, *Nat. Methods* 12 (5) (2015) 453–457.
- [23] R. Xu, J. Wu, X. Zhang, et al., Modified Bu-zhong-yi-qi decoction synergies with 5 fluorouracil to inhibit gastric cancer progress via PD-1/PD-L1-dependent T cell immunization, *Pharmacol. Res.* 152 (2020) 104623.
- [24] A. Sveen, S. Kopetz, R.A. Lothe, Biomarker-guided therapy for colorectal cancer: strength in complexity, *Nat. Rev. Clin. Oncol.* 17 (1) (2020) 11–32.
- [25] J. He, W. Liu, Identification of disrupted pathways associated with colon cancer based on combining protein-protein interactions and pathway data, *J. Cancer Res. Therapeut.* 14 (Supplement) (2018) S998–S1003.
- [26] R. Bajo-Gráneras, J. Crespo-Sanjuán, R.M. García-Centeno, et al., Expression and potential role of apolipoprotein D on the death survival balance of human colorectal cancer cells under oxidative stress conditions, *Int. J. Colorectal Dis.* 28 (6) (2013) 751–766.
- [27] Y. Zhou, J.K. Shen, Z. Yu, et al., Expression and therapeutic implications of cyclin-dependent kinase 4 (CDK4) in osteosarcoma, *Biochim. Biophys. Acta, Mol. Basis Dis.* 1864 (5 Pt A) (2018) 1573–1582.
- [28] F. Liu, W. Liu, S. Zhou, et al., Identification of FABP5 as an immunometabolic marker in human hepatocellular carcinoma, *J. Immunother. Cancer* 8 (2) (2020) e000501.
- [29] F. Liu, W. Liu, S. Zhou, et al., Identification of FABP5 as an immunometabolic marker in human hepatocellular carcinoma, *J. Immunother. Cancer* 8 (2) (2020) e000501.
- [30] K.C. Park, J. Paluncic, Z. Kovacevic, et al., Pharmacological targeting and the diverse functions of the metastasis suppressor, NDRG1, in cancer, *Free Radic. Biol. Med.* 157 (2020) 154–175.
- [31] E.S. Villodre, X. Hu, B.L. Eckhardt, et al., NDRG1 in aggressive breast cancer progression and brain metastasis, *J. Natl. Cancer Inst.* 114 (4) (2022) 579–591.
- [32] D. Elias, H.J. Ditzel, Fyn is an important molecule in cancer pathogenesis and drug resistance, *Pharmacol. Res.* 100 (2015) 250–254.
- [33] J. Yu, Z. Zhou, Z. Wei, et al., FYN promotes gastric cancer metastasis by activating STAT3-mediated epithelial-mesenchymal transition, *Transl. Oncol* 13 (11) (2020) 100841.
- [34] Y. Tian, H. Xu, A.A. Farooq, et al., Maslinic acid induces autophagy by down-regulating HSPA8 in pancreatic cancer cells, *Phytother. Res.* 32 (7) (2018) 1320–1331.
- [35] I.W. Cheuk, M.T. Siu, J.C. Ho, et al., ITGAV targeting as a therapeutic approach for treatment of metastatic breast cancer, *Am. J. Cancer Res.* 10 (1) (2020) 211–223.
- [36] X. You, M. Li, H. Cai, et al., Calcium binding protein S100A16 expedites proliferation, invasion and epithelial-mesenchymal transition process in gastric cancer, *Front. Cell Dev. Biol.* 9 (2021) 736929. Published 2021 Sep. 28.
- [37] M. Liang, W. Yao, B. Shi, et al., Circular RNA hsa_circ_01110389 promotes gastric cancer progression through upregulating SORT1 via sponging miR-127-5p and miR-136-5p, *Cell Death Dis.* 12 (7) (2021) 639. Published 2021 Jun 23.
- [38] Q. Li, X. Zhou, Z. Fang, Z. Pan, Effect of STC2 gene silencing on colorectal cancer cells, *Mol. Med. Rep.* 20 (2) (2019) 977–984.
- [39] S. Chen, M. Yu, L. Ju, et al., The immune-related biomarker TEK inhibits the development of clear cell renal cell carcinoma (ccRCC) by regulating AKT phosphorylation, *Cancer Cell Int.* 21 (1) (2021) 119. Published 2021 Feb 18.
- [40] F. Luan, X. Li, X. Cheng, et al., TNFRSF11B activates Wnt/ β -catenin signaling and promotes gastric cancer progression, *Int. J. Biol. Sci.* 16 (11) (2020) 1956–1971.
- [41] B. Rowshanravan, N. Halliday, D.M. Sansom, CTLA-4: a moving target in immunotherapy, *Blood* 131 (1) (2018) 58–67.
- [42] H. Lingel, M.C. Brunner-Weinzler, CTLA-4 (CD152): a versatile receptor for immune-based therapy, *Semin. Immunol.* 42 (2019) 101298.
- [43] X. Hu, Z. Lin, Z. Wang, et al., Emerging role of PD-L1 modification in cancer immunotherapy, *Am. J. Cancer Res.* 11 (8) (2021) 3832–3840.
- [44] D.C. Hinshaw, L.A. Shevde, The tumor microenvironment innately modulates cancer progression, *Cancer Res.* 79 (18) (2019) 4557–4566.
- [45] S. Xiong, L. Dong, L. Cheng, Neutrophils in cancer carcinogenesis and metastasis, *J. Hematol. Oncol.* 14 (1) (2021) 173. Published 2021 Oct 21.
- [46] P. Ge, W. Wang, L. Li, et al., Profiles of immune cell infiltration and immune-related genes in the tumor microenvironment of colorectal cancer, *Biomed. Pharmacother.* 118 (2019) 109228.
- [47] S. Liu, A. Song, Y. Wu, et al., Analysis of genomics and immune infiltration patterns of epithelial-mesenchymal transition related to metastatic breast cancer to bone, *Transl. Oncol* 14 (2) (2021) 100993.
- [48] D. Kumar, Y. Romero, K.N. Schuck, et al., Drivers and regulators of humoral innate immune responses to infection and cancer, *Mol. Immunol.* 121 (2020) 99–110.
- [49] Y. Kurebayashi, H. Ojima, H. Tsujikawa, et al., Landscape of immune microenvironment in hepatocellular carcinoma and its additional impact on histological and molecular classification, *Hepatology* 68 (3) (2018) 1025–1041.
- [50] K. Lei, A. Kurum, M. Kaynak, et al., Cancer-cell stiffening via cholesterol depletion enhances adoptive T-cell immunotherapy, *Nat. Biomed. Eng.* 5 (12) (2021) 1411–1425.
- [51] W. Li, J. Zeng, B. Luo, et al., [High expression of activated CD4+ memory T cells and CD8+ T cells and low expression of M0 macrophage are associated with better clinical prognosis in bladder cancer patients], *Xi Bao Yu Fen Zi Mian Yi Xue Za Zhi* 36 (2) (2020 Feb) 97–103.